Journal of The Electrochemical Society, **152** (6) B193-B197 (2005)
0013-4651/2005/152(6)/B193/5/$7.00 © The Electrochemical Society, Inc.

Voltammetry and Impedance Studies of Ta in Aqueous HF

Sanjeev Sapra, Hongqi Li, Zuocheng Wang, and Ian Ivar Suni*,z

[a]*Department of Chemical Engineering, Center for Advanced Materials Processing, Clarkson University, Potsdam, New York 13699-5705, USA*

Tantalum (Ta) electrochemistry is studied in aqueous HF and NH_4F by cyclic voltammetry and electrochemical impedance spectroscopy. The much greater hydrogen evolution current and the much lower charge-transfer resistance for the high-frequency impedance loop in HF relative to NH_4F demonstrate that the native Ta_2O_5 film dissolves in HF, but not in NH_4F. Weight loss experiments and cyclic voltammetry demonstrate that at cathodic potentials in aqueous HF, dissolution of Ta oxide allows electrochemical dissolution of the exposed surface into Ta^{5+}. In addition, unusual low frequency impedance behavior is seen for Ta in HF analogous to that reported by Bojinov for several different metal surfaces at anodic potentials in concentrated acids. This suggests the presence of an ultrathin, passive film in HF and is consistent with the poor adhesion often obtained for Cu electrodeposition onto Ta. This passive film may correspond to the Ta suboxide (TaO) previously observed by X-ray photoelectron spectroscopy at the Ta/Ta_2O_5 interface.
 [DOI: 10.1149/1.1899286]

Manuscript submitted June 10, 2004; revised manuscript received December 15, 2004. Available electronically May 4, 2005.

Diffusion barriers have been required for Si-based semiconductor devices since the introduction of Cu, a deep level defect, as the interconnect material during the late 1990s. Ti/TiN and Ta/TaN materials have been widely employed as diffusion barriers and will likely remain viable for the 90 and 65 nm technology nodes.[1] The relatively high resistivity of these materials requires the deposition of a Cu seed layer prior to Cu electrodeposition.[2] Both barrier and seed layers are usually deposited by a mixed plasma/physical vapor deposition (PVD) process known as either ionized physical vapor deposition (I-PVD) or ion metal plasma (IMP).[3-5] However, electrochemical deposition would provide large cost reductions during this step in microelectronic device fabrication.

A variety of all-electrochemical methods, including Pd seeding followed by electroless Cu deposition, are currently under development for deposition of Cu seed layers atop barrier materials for Si-based semiconductor devices.[6] Many of these methods employ aqueous HF or NH_4F for oxide removal either prior to or during seeding or deposition onto both Ti/TiN[7-9] and Ta/TaN[10-17] diffusion barriers. Fluoroborate solutions, in which HF can form following disproportionation, have also been proposed for minimizing oxide formation.[18]

However, few studies have been published of the nature of the electrochemical interface that exists at these diffusion barrier materials in aqueous HF.[19] This might be considered surprising, given the critical dependence of adhesion on interfacial impurities such as oxide films.[20] It should be noted that extensive electrochemical studies have been reported for a closely similar system, Nb in aqueous HF.[21,22] This report describes cyclic voltammetry (CV), electrochemical impedance spectroscopy (EIS), and atomic force microscopy (AFM) studies of the Ta-HF aqueous interface. These demonstrate that the Ta native oxide film can indeed be removed in aqueous HF. However, unusual low-frequency behavior seen in EIS studies is consistent with the existence of an ultrathin, passive film at the Ta/HF interface. In addition, depending on the potential and pH, Ta oxide dissolution may be accompanied by simultaneous Ta dissolution.

Experimental

A saturated calomel (SCE) reference electrode, Pt spiral and Ag sheet counter electrodes, and 99.9% pure embedded Ta disk and Ta sheet working electrodes were employed. CV experiments were conducted using both an EG&G/PAR model 263A-1 potentiostat/galvanostat and a Bioanalytical Systems (BAS) model 100B/W electrochemical workstation. EIS was performed using the ac impedance module of the BAS electrochemical workstation, which applies multisine waveforms and fast Fourier transform analyses to obtain EIS data over the frequency range 10^{-2}-10^{3} Hz. Reported results employ a 5 mV ac probe voltage, with linearity demonstrated by the invariance of the results to the exact probe voltage.

The impedance results that are given below were obtained by immersing the Ta electrode into semiconductor-grade HF/NH_4F diluted with triply-distilled water, then holding the Ta electrode at the potential of interest until steady-state conditions are attained, as seen by impedance measurements. Steady-state conditions were attained rapidly at all potentials except for −550 mV SCE, where the steady state was not attained until after approximately 90 min. Unless otherwise noted, all electrolytes were continuously deaerated with Ar. However, Ar deaeration does not have a significant effect on the measured impedance spectrum. Following the attainment of steady-state conditions, surface roughness was measured on 99.9% pure Ta foil using a Digital Instruments Bioscope BS-3-Z AFM.

Results and Discussion

Figure 1 shows cyclic voltammetry of a Ta disk electrode in 2.5 M HF, 1.25 M HF/1.25 M NH_4F, and 2.5 M NH_4F, starting from the most anodic potential, then scanning to the most cathodic potential and back. The two highest current peaks both correspond to 2.5 M HF, with the higher peak associated with the voltage scan in the anoodic direction. In 2.5 M HF, Ta oxide formation begins at approximately +300 mV SCE. Relative to the other two electrolytes, the current measured in 2.5 M NH_4F is insignificant. Weight loss experiments on the Ta sheet demonstrate that the anodic peaks seen in 2.5 M HF and 1.25 M HF/1.25 M NH_4F at approximately −420 mV SCE can be attributed to Ta dissolution into the Ta^{5+} oxidation state. The solution-phase species is likely TaF_7^{2-}, found in commercial Ta salts.

These anodic current peaks probably correspond to the active-passive transition seen in many metals immersed in concentrated acidic electrolytes in which a thin passive film is formed at highly anodic potentials. Similar anodic current peaks are observed for the similar system, Nb in aqueous HF.[21,22] Below about −600 mV (−700 mV) SCE in 2.5 M HF (1.25 M HF/1.25 M NH_4F), hydrogen evolution occurs. In addition to other evidence discussed below, the lack of significant hydrogen evolution in 2.5 M NH_4F provides evidence that bare Ta metal is not exposed in this electrolyte.

These cyclic voltammograms can be understood qualitatively from the following reactions[23]

$$Ta_2O_5 + 10H^+ + 10e^- \rightleftarrows 2Ta + 5H_2O \quad [1]$$

$$TaF_7^{2-} + 5e^- \rightleftarrows Ta + 7F^- \quad [2]$$

The best available standard reduction potentials for these two reactions are about −0.81 and −0.45 V SCE, respectively.[23] The latter value corresponds approximately to the potential at which Ta disso-

* Electrochemical Society Active Member.
z E-mail: isuni@clarkson.edu

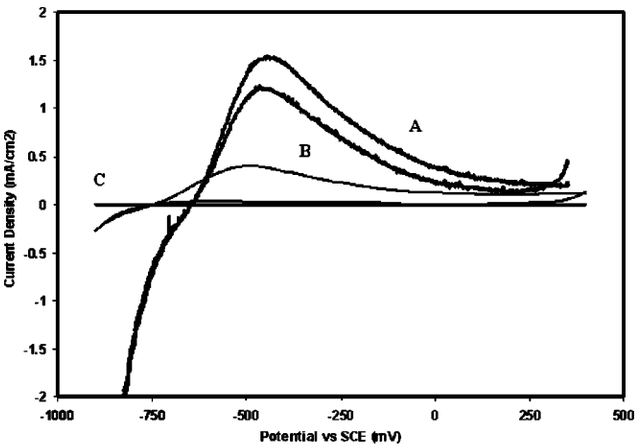

Figure 1. Cyclic voltammograms for Ta in 2.5 M HF (A), 1.25 *M* HF/1.25 M NH_4F (B), and 2.5 M NH_4F (C) at a scan rate of 10 mV/s.

lution into TaF_7^{2-} occurs in Fig. 1. In this report, the upward sloping side of the anodic current peak is attributed to active Ta dissolution arising from Eq. 2. On the other hand, the downward sloping side of the anodic current peaks corresponds in part to Ta passive film or Ta oxide formation arising from Eq. 1. At more anodic potentials, the moderate anodic currents likely reflect a steady-state condition whereby Ta passive film forms at the Ta/film interface, while the Ta passive film dissolves at the film/electrolyte interface. A similar interpretation has been put forward for Nb in aqueous HF. The Pourbaix diagram created from these standard reduction potentials for 1.0 M F^- is shown in Fig. 2. The solution-phase specie shown is the thermodynamically stable specie in equilibrium, assumed to be at unit activity. For the sake of simplicity, this assumes complete dissociation of HF and neglects formation of HF_2^- and higher-order HF polymers.[24,25] Polymer formation is unlikely at the moderate HF concentrations considered here. The voltammetry and impedance results discussed below suggest that the pH at which the Ta native oxide can be removed is not as extreme as is indicated in Fig. 2.

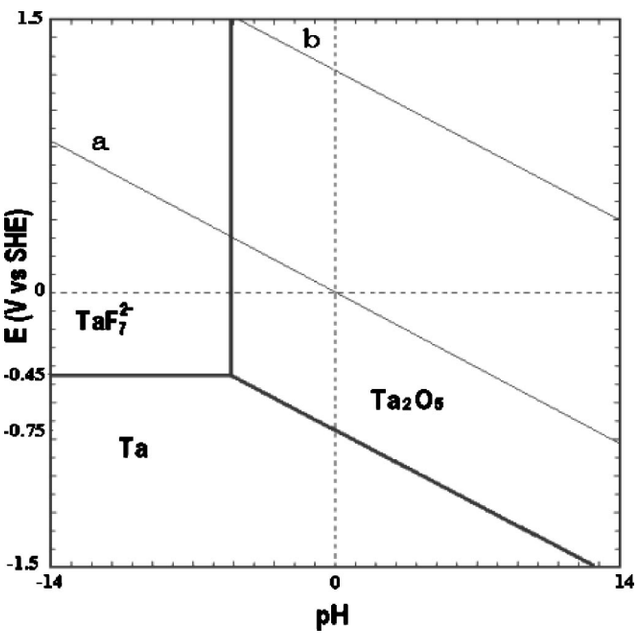

Figure 2. Pourbaix diagram for Ta in 1.0 M HF.

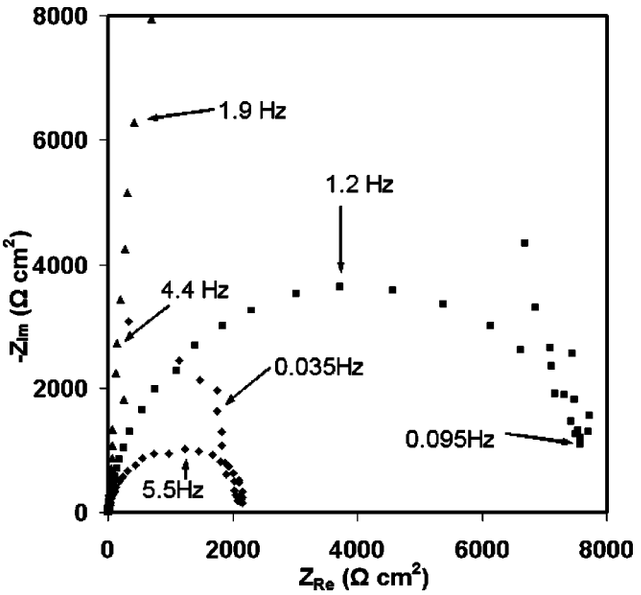

Figure 3. Nyquist representations for the impedance spectra ranging from 10^{-2} to 10^3 Hz at +200 mV in (a) 2.5 M HF (♦), (b) 1.25 M HF/1.25 M NH_4F (■), and (c) 2.5 M NH_4F (●).

However, the accuracy of the standard reduction potentials quoted above is not addressed in this study.

According to this simplified Pourbaix diagram, Ta oxide formation can only be prevented at highly cathodic potentials or extremely low pH. Ideally, for Ta oxide removal or for direct electroless or electrodeposition onto Ta, a stable bare Ta metal surface is needed at a potential at which hydrogen evolution does not occur. However, at all cathodic potentials and electrolyte concentrations investigated here, either the Ta surface is oxidized, hydrogen evolution occurs, or Ta dissolution occurs. One conclusion from these investigations is that while HF can dissolve the native oxide from Ta, care must be taken to prevent excessive Ta dissolution and to prevent hydrogen incorporation into electrodeposits. The largest Ta dissolution current in Fig. 1 (1.5 mA/cm^2) corresponds to a Ta dissolution rate of about 20 nm/min. It should be noted that this is simply an example calculation, since the anodic currents observed in Fig. 1 are close to but not exactly equal to steady-state currents, as exhibited by the difference between the forward and reverse scans.

The nature of the Ta electrochemical interface was further investigated using electrochemical impedance spectroscopy (EIS), with a particular emphasis on the 2.5 M HF electrolyte, in which oxide removal should be most complete. Impedance is one of the few techniques capable of *in situ* studies of surface oxidation. Most potential *ex situ* probes suffer from the possibility of facile surface oxidation during sample transfer to a vacuum environment. Nyquist representations of the impedance results in all three electrolytes at +200 mV SCE are given in Fig. 3, and Nyquist representations of the impedance results at a variety of potentials in 2.5 M HF are shown in Fig. 4. In most cases, the high-frequency data appear as a depressed semicircle and can be fitted to a variation of the Randles model for an electrochemical interface, replacing the double-layer capacitance with a constant phase element (CPE)

$$Z_{\mathrm{CPE}} = \frac{1}{T(j\omega)^{\phi}} \qquad [3]$$

When ϕ is unity, the CPE reduces to a simple capacitance. The most common explanation for the existence of a CPE at a solid electrode surface is surface inhomogeneity arising from surface roughness or from chemical inhomogeneity.[26] The best-fit values for R_{ct}, T, ϕ, and R_{s} corresponding to the high-frequency data for the different

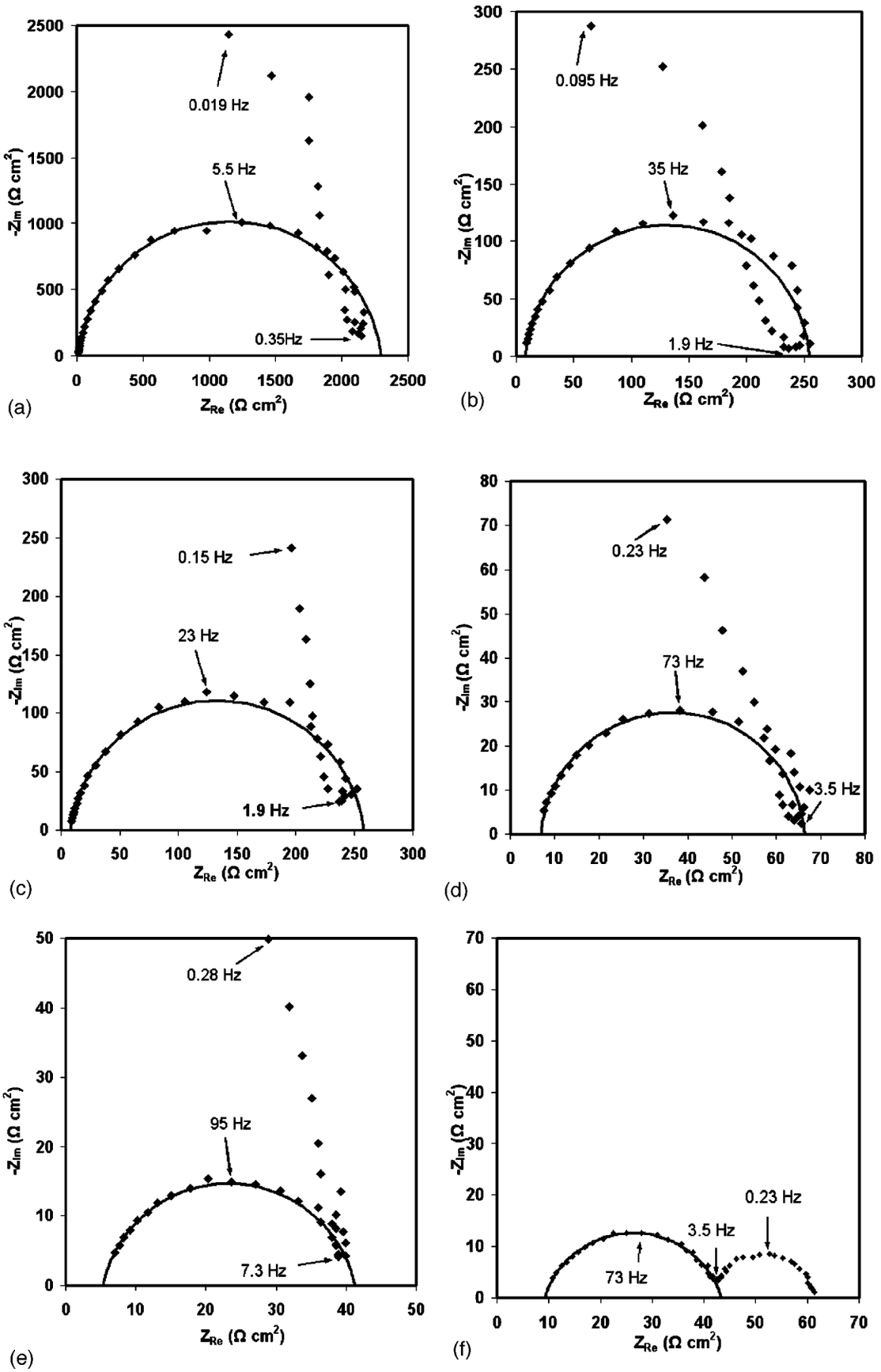

Figure 4. Nyquist representations for the impedance spectra ranging from 10^{-2} Hz to 10^{3} Hz in 2.5 *M* HF at (a, top left) 200, (b, top right) 50, (c, center left) −100, (d, center right) −250, (e, bottom left) −400, (f, bottom right) −550 mV *vs.* SCE.

Table I. Best-fit Impedance parameters for Ta at +200 mV *vs.* SCE.

Electrolyte	R_{ct} (Ω cm^2)	T (μF s$^{\phi-1}$ cm^{-2})	ϕ	R_s (Ω cm^2)
2.5 M HF	2.3×10^3	15	0.93	9.8
1.25 M HF + 1.25 M NH_4F	8.0×10^3	20	0.94	3.8
2.5 M NH_4F	3.5×10^6	15	0.96	3.8

electrolytes and potentials that were investigated are given in Tables I and II.

The values given in Tables I and II for the magnitude of the CPE can be compared to those expected for bare metal and oxidized metal surfaces. The relationship between the magnitude of a CPE and the double-layer capacitance at a metal electrode is quite complex and has been extensively studied.[27-29] The existence of a CPE rather than a simple capacitance is generally ascribed to surface heterogeneity, although the relative importance of geometric surface roughness and adsorption effects is not always clear. Thus, the magnitude of the CPE corresponds reasonably well to a capacitance value only for the results in Table I, where the CPE exponent is close to unity. Published impedance studies of the Ta native oxide report a differential capacitance of approximately 14 μF/cm^2.[30] This was attributed to two capacitances in series, the Hemlholtz capacitance at the Ta/electrolyte interface and the Ta oxide capacitance. However, this value for the differential capacitance is not significantly different from the canonical value for the Helmholtz capacitance (20 μF/cm^2) often assumed for the solid/electrolyte interface, so the oxide contribution to this capacitance cannot be accurately determined.

The magnitudes of the CPE in Table II can also be compared to canonical values for the Helmholtz capacitance, although as discussed above, this comparison is not quantitative due to the significant deviation of ϕ from unity in some cases. As the potential becomes more cathodic, the deviation of ϕ from unity increases, along with the magnitude of the CPE, which reaches values much greater than 20 μF/cm^2. Qualitatively, the corresponding increase in the interfacial capacitance is most likely associated with an increase in the surface roughness. This suggests that the anodic currents arising from Ta dissolution at cathodic potentials in Fig. 1 cause an increased surface roughness. Alternatively, one might view this as arising from oxide-induced smoothing of the electrode surface, as is known to occur on valve metals. The surface roughness of the Ta sheet was also measured by atomic force microscopy (AFM), and these results are also included in Table II. As expected, the surface roughness increases at more cathodic potentials. For the different reasons discussed above, while the differential capacitance values given in Tables I and II demonstrate that in no case is the Ta surface covered by an oxide thicker than the native oxide, they cannot distinguish between a bare Ta surface and a Ta surface covered with a thin oxide or other passive film.

The continuous increase in the charge-transfer resistance with increasing potential in Table II supports the hypothesis that the Ta electrode becomes covered by a passive or oxide film at anodic potentials. In general, the interfacial charge-transfer resistance appears to provide greater insight into the extent to which the surface is covered by a passive film than does the interfacial capacitance.

Table II. Best-fit impedance parameters for Ta in 2.5 M HF.

Potential (mV *vs.* SCE)	R_{ct} (Ω cm^2)	T (μF s$^{\phi-1}$ cm^{-2})	ϕ	R_s (Ω cm^2)	σ_{rms} (nm)
−550	34	180	0.81	9.2	11.2
−400	36	103	0.87	5.3	8.6
−250	59	46	0.95	6.9	-
−100	250	43	0.92	8.0	7.7
+50	250	22	0.95	8.1	-
+200	2.3×10^3	15	0.93	9.8	6.6

This is best demonstrated by impedance studies of Ta at +200 mV SCE in 2.5 M HF, 1.25 M HF/1.25 M NH_4F, and 2.5 M NH_4F presented in Fig. 3, with best-fit values for the high frequency impedance data in Table I. The charge-transfer resistance in 2.5 M NH_4F is several orders of magnitude higher than in 2.5 M HF, indicating that the Ta surface is oxidized in 2.5 M NH_4F, but not in 2.5 M HF. This reasoning is consistent with the large difference in the extent of hydrogen evolution seen at highly cathodic potentials in Fig. 1. The extent of hydrogen evolution in 2.5 M HF is far greater than that in 2.5 M NH_4F, and only in 2.5 M HF does the rate of hydrogen evolution accelerate dramatically at highly cathodic potentials, as typically seen on bare metal electrodes in acidic media.

The low-frequency impedance behavior shown in Fig. 3 and 4 is unexpected for this system and is not analyzed quantitatively. However, these results are qualitatively similar to those seen by Bojinov and co-workers for anodic films on metal electrodes immersed in highly acidic electrolytes.[31-34] Such unusual low-frequency behavior is often referred to as an inductive loop and likely originates from low-frequency growth/dissolution of an oxide or passive film. An alternative and sometimes equivalent explanation is the existence of multistep reactions involving adsorbed intermediates.[26] The existence of these low-frequency loops appears to indicate that although the native Ta oxide is dissolved at cathodic potentials in 2.5 M HF, a thin conductive film likely exists. This is consistent with the poor adhesion that often plagues direct electrodeposition of Cu onto Ta from HF electrolytes.

The Pourbaix diagram from Fig. 2 does not include the possible existence of a Ta suboxide, similar to that found at the interface between Si and its native oxide. The structure of native Ta oxide has been studied using X-ray photoelectron spectroscopy (XPS), revealing an interfacial TaO suboxide beneath a 2-3 nm Ta_2O_5 layer.[35,36] The TaO suboxide may form islands at the Ta/Ta_2O_5 interface.[35] As discussed above, the contribution of this interfacial suboxide to the differential capacitance is too small to distinguish from the Helmholtz capacitance, whose exact value is somewhat uncertain and is in this case convoluted with the surface roughness. Such an interfacial TaO film or TaO island film may be responsible for the unusual low-frequency impedance behavior seen in the current study.

Acknowledgments

This research has been supported by National Science Foundation grant CTS-0094773 and the Center for Advanced Materials Processing (CAMP) at Clarkson University. Thanks to Dipankar Roy for helpful discussions and to Anja Mueller for use of her AFM.

Clarkson University assisted in meeting the publication costs of this article.

References

1. L. Peters, *Semicond. Int.*, **26**, 50 (2003).
2. K. M. Takahashi, *J. Electrochem. Soc.*, **147**, 1414 (2000).
3. B. Chin, P. Ding, B. Sun, T. Chiang, D. Angelo, I. Hashim, Z. Xu, S. Edelstein, and F. Chen, *Solid State Technol.*, **41**, 141 (1998).
4. E. K. Broadbent, E. J. McInerny, L. A. Gochberg, and R. L. Jackson, *J. Vac. Sci. Technol. B*, **7**, 258 (1999).
5. E. C. Cooney, D. C. Strippe, and J. W. Korejwa, *J. Vac. Sci. Technol. A*, **18**, 1550 (2000).
6. http://public.itrs.net/Files/2003ITRS/Home2003.htm
7. Y. Shacham-Diamand and V. M. Dubin, *Microelectron. Eng.*, **33**, 47 (1998).
8. J. J. Kim, S. K. Kim, C. H. Lee, and Y. S. Kim, *J. Vac. Sci. Technol. B*, **21**, 33 (2003).
9. J. J. Kim, S. H. Cha, and Y. S. Lee, *Jpn. J. Appl. Phys., Part 2*, **42**, L953 (2003).
10. S. W. Hong and J. W. Park, *Electrochem. Solid-State Lett.*, **5**, C107 (2002).
11. S. W. Hong, Y. S. Lee, and J. W. Park, *Electrochem. Solid-State Lett.*, **6**, C12

(2003).
12. H. H. Hsu, C. W. Teng, S. J. Lin, and J. W. Yeh, *J. Electrochem. Soc.*, **149**, C143 (2002).
13. S. Y. Chang, C. J. Hsu, R. H. Fang, and S. J. Lin, *J. Electrochem. Soc.*, **150**, C603 (2003).
14. H. H. Hsu, J. W. Yeh, and S. J. Lin, *J. Electrochem. Soc.*, **150**, C813 (2003).
15. Z. Wang, T. Ida, H. Sakaue, S. Shingubara, and T. Takahagi, *Electrochem. Solid-State Lett.*, **6**, C38 (2003).
16. Z. Wang, H. Sakaue, S. Shingubara, and T. Takahagi, *Jpn. J. Appl. Phys., Part 1*, **42**, 1843 (2003).
17. Z. Wang, H. Li, H. H. Shodiev, and I. I. Suni, *Electrochem. Solid-State Lett.*, **7**, C67 (2004).
18. A. Radisic, Y. Cao, P. Taephaisitphongse, A. C. West, and P. C. Searson, *J. Electrochem. Soc.*, **150**, C362 (2003).
19. P. J. S. Mangat, W. J. Dauksher, R. Whig, and W. L. O'Brien, *J. Vac. Sci. Technol. A*, **18**, 1211 (2000).
20. L. Chen, N. Magtoto, B. Erkstrom, and J. Kelber, *Thin Solid Films*, **376**, 115 (2000).
21. S. Cattarin, M. Musiani, and B. Tribollet, *J. Electrochem. Soc.*, **149**, B457 (2002).
22. M. Bojinov, S. Cattarin, M. Musiani, and B. Tribollet, *Electrochim. Acta*, **48**, 4107 (2003).
23. *Standard Potentials in Aqueous Solution*, A. J. Bard, R. Parsons, and J. Jordan, Editors, Marcel Dekker, New York (1985).
24. P. McTigue, T. A. O'Donnell, and B. Verity, *Aust. J. Chem.*, **38**, 1797 (1985) And references therein.
25. R. Braddy, P. T. McTigue, and B. Verity, *J. Fluorine Chem.*, **66**, 63 (1994).
26. A. Lasia, in *Modern Aspects of Electrochemistry*, B. E. Conway, J. O'M. Bockris, and R. E. White, Editors, p. 143, Kluwer/Plenum, New York (1999).
27. G. J. Brug, A. L. G. van den Eeden, M. Sluyters-Rehbach, and J. H. Sluyters, *J. Electroanal. Chem. Interfacial Electrochem.*, **176**, 275 (1984).
28. T. Pajkossy, *J. Electroanal. Chem.*, **364**, 111 (1994).
29. E. Lust, A. Janes, K. Lust, V. Sammelselg, and P. Miidla, *Electrochim. Acta*, **42**, 2861 (1997).
30. O. Kerrec, D. Devilliers, H. Groult, and M. Chemla, *Electrochim. Acta*, **40**, 719 (1995).
31. M. Bojinov, *J. Electroanal. Chem.*, **405**, 15 (1996).
32. M. Bojinov, G. Fabricius, T. Laitinen, and T. Saario, *Electrochim. Acta*, **44**, 4331 (1999).
33. M. Bojinov, I. Betova, G. Fabricius, T. Laitinen, and R. Raicheff, *J. Electroanal. Chem.*, **475**, 58 (1999).
34. M. Bojinov and T. Tzvetkoff, *J. Phys. Chem. B*, **107**, 5101 (2003).
35. S. Lecuyer, A. Quemerais, and G. Jezequel, *Surf. Interface Anal.*, **18**, 257 (1992).
36. O. Kerrec, D. Devilliers, H. Groult, and P. Marcus, *Mater. Sci. Eng., B*, **55**, 134 (1998).